Tunable acoustic labyrinthine acoustic metamaterials for broadband noise absorption

Abbas Dalvand
K.N. Toosi University of Technology
a.dalvand@email.kntu.ac.ir

Reza Hedayati
K.N. Toosi University of Technology
rezahedayti@kntu.ac.ir

Aliasghar Jafari
K.N. Toosi University of Technology
ajafari@kntu.ac.ir

Abstract

This study introduces the Adjustable Acoustic Labyrinth Metamaterial (AALM) as a novel solution for noise pollution, particularly for managing the unpredictable and shifting frequencies produced by vehicles and mechanical equipment. The AALM is an adaptable metamaterial that integrates labyrinth structures with Helmholtz resonators (HR) to deliver highly tunable sound absorption. The system's adaptability stems from two adjustable parameters: the number of active labyrinthine canals and the cross-sectional area of the wave entrance. This dual-control mechanism provides remarkable flexibility. By altering the quantity of coiled spaces, users can achieve major frequency adjustments of approximately 120 Hz. For fine-tuning, modifying the wave entrance allows for minor adjustments of about 10 Hz at low frequencies and up to 50 Hz at higher frequencies. This tunability enables the AALM to operate effectively across a broad spectrum from approximately 220 Hz to 2000 Hz, which covers a significant portion of the primary target range for noise control (100-2000 Hz). In total, the system offers 24 distinct operational modes, capable of producing 36 different absorption peaks that are near-perfect, especially in the low-frequency range. This makes the AALM a highly promising technology for advanced acoustic management.

1. Introduction

In the modern landscape of technological advancements, the prevalence of complex noise generation sources in automotive, manufacturing, and aerospace industries has made noise reduction an increasingly significant topic for researchers [1-6]. To address this issue, researchers have proposed several solutions including making use of acoustic foams and acoustic metamaterials [7-11].

Porous materials exhibit excellent sound absorption in the mid to high-frequency range [12, 13]. However, they perform poorly in low frequencies, and they must be produced at dimensions comparable to the operational wavelength [14, 15]. Micro-perforated panels (MPPs) present another effective solution for sound absorption [16]. They are particularly advantageous for controlling sound energy at low frequencies. However, their efficiency in low-frequency absorption necessitates a large physical air cavity, which is often impractical due to geometric constraints [17, 18]. Traditional Helmholtz resonators (HR) have also been a promising concept among sound absorption methods [19].

Despite various advancements, achieving low-frequency sound absorption with a wide bandwidth remains a significant challenge. To address this, acoustic metamaterials have been developed, demonstrating enormous potential for effective low-frequency sound absorption [20, 21]. Acoustic metamaterials are artificially engineered periodic structures, primarily composed of locally resonant sub-wavelength components, that present unique behaviors. Metamaterial-based sound absorbers exhibit exceptional performance in the low-frequency range by enhancing sound-matter interactions that are unattainable with natural materials [22, 23]. Also, they can lead to some unusual properties such as anomalous refraction, subwavelength imagining, cloaking, and negative values of density, Poisson's ratio and Young's modulus [24-28]. One of the efficient types of acoustic metamaterial is coiled-up space or labyrinthine structures in which viscous-thermal characteristics affect the sound propagation in small spaces [29]. Labyrinthine Acoustic Metamaterials (LAMMs), characterized by their intricate curled perforations, stand out as one of the most impactful types of acoustic metamaterials due to their exceptional constitutive parameters and wide range of potential applications. LAMMs can exhibit a range of remarkable properties, such as double negativity, near-zero density, and a high refractive index across various

frequencies. These characteristics lead to intriguing phenomena such as negative refraction and zero-density tunneling [30-32].

Resonators are typically designed based on quarter-wavelength principles, which result in significant thickness in conventional resonators. However, coiled-up space can achieve the resonance effect without substantially increasing the thickness [33]. The wave path can be extended in directions other than thickness, making this approach common in Fabry-Perot (FP) type channels [34]. The advancements in additive manufacturing have significantly increased the popularity of labyrinthine structures. This is due to the fact that their production using traditional methods was challenging and time-consuming [35-37].

Noise occurs across a range of frequencies, necessitating a tunable response system for effective noise reduction. One such system is Active Noise Control (ANC), which employs microphones to detect noise frequencies and speakers to produce inverse sound waves of the same frequency [38, 39]. Despite its high efficacy, this method requires precise control systems and is often costly. Alternatively, innovative mixtures of metamaterials can be employed to achieve wide-band sound absorption. Utilizing multiple Helmholtz resonators with varying neck and cavity sizes within a single structure induces resonance across different frequencies, resulting in highly effective sound absorption [40].

Utilizing Micro-perforated Panels (MPPs) in conjunction with coiled-up metamaterials results in wider bandwidth sound absorption. This demonstrates that the acoustic impedance at the point of wave entry significantly influences the acoustic absorption characteristics. Additionally, modifying the shape of these structures alters the broadband absorption, with slit-shaped designs exhibiting superior performance compared to square and circular configurations [41]. In improved results, the parallel labyrinthine structure has been employed with MPPs to not only reduce the frequency of maximum absorption but to also enhance the absorption bandwidth [29]. In another approach, researchers have enthusiastically explored the potential of labyrinthine structures combined with porous media. This is due to their quasi-perfect sound absorption capabilities at low frequencies and their acceptable acoustic absorption across a wide frequency band. This model has been developed as an effective method for noise reduction [42, 43]. However, fabricating porous materials in a labyrinthine form is challenging and expensive, and these structures are not easily adjustable for different frequencies. Additionally, it is sometimes essential to hear specific

sounds. For instance, in the automotive industry, detecting sounds such as bicycle bells, children playing, or sirens from approaching emergency vehicles is crucial for safety [44]. Porous media do not possess this capability.

With changes in geometry, some properties of conventional passive metamaterials such as bulk modulus and density can be changed, which in turn results in change the interest frequency for sound absorption [45]. The inherent scalability of active metamaterials for a wide range of applications, makes them a versatile and adaptable solution in various fields of study and industry [46].

This study puts forward and evaluates an innovative device, the Adjustable Acoustic Labyrinthine Metamaterial (AALM), designed to deliver highly adaptable sound absorption. The primary goal is to create a single, tunable structure that demonstrates superior absorption efficiency across the broad frequency spectrum of 200-2000 Hz. The AALM's performance represents a significant advancement, providing consistently high absorption coefficients across its operational range. This capability overcomes the core limitations of both traditional passive metamaterials, known for their narrow frequency-specific performance, and porous materials, which typically offer broad but only moderate absorption.

The adaptable sensitivity of the AALM makes it an ideal solution for dynamic noise environments where frequencies fluctuate, such as in automotive applications. This functionality is achieved through two physical control mechanisms: altering the position of the wave entrance, or "window," and adjusting a metal plate that governs the number of active channels within the labyrinth structure. This approach addresses a central challenge in the cutting-edge field of active metamaterials, which is the ongoing effort to increase the number of operational modes to cover a wider range of frequencies [44].

To validate the proposed design, this research employs a dual methodology, combining numerical analyses within the COMSOL Multiphysics software with physical experiments conducted in an impedance tube setup. The investigation includes a detailed discussion of the AALM's different operational modes and their respective performance levels, an examination of wave propagation within the labyrinth, and an identification of potential obstacles that could hinder optimal acoustic performance.

2. Materials and methods

This study introduces the Adjustable Acoustic Labyrinthine Metamaterial (AALM), a sound absorber built from a rigid structure containing six coiled-up spaces with a constant rectangular cross-section. The device's innovation lies in its dual-system control, which allows for tunable acoustic properties.

As shown in Figure 1, the first control mechanism is a movable window that modifies the cross-sectional area of the wave entrance. The second mechanism, detailed in Figure 1(b), is a rigid metal plate located in the middle of the structure. By moving this plate, the number of active coiled-up channels within the labyrinth can be changed. Consequently, these two systems—the window adjusting the entrance area and the plate altering the number of pathways—work together to control the propagation of sound waves.

The underlying principle of the labyrinthine design is to achieve optimal sound absorption in a compact, rigid device by increasing the effective length of the acoustic path. This approach makes it particularly effective for absorbing sound at low frequencies, where wavelengths can be in the 1-2 meter range.

Figure 1: Schematic of (a) window and (b) cell

2.1. Numerical modelling

The numerical analysis of the AALM was done using Finite Element Method (FEM) performed in COMSOL Multiphysics 6.2. In the numerical model, a complete simulation of wave propagation was developed by modelling the interaction between two physics: Pressure Acoustics and Thermoviscous Acoustics. The analysis was conducted in the frequency domain of 60-2000 Hz, with a plane wave of magnitude $P_0 = 1\ Pa$ applied at the port boundary. Figure 2 demonstrates the 3D model discretization, sound boundary wall conditions, and different domains. Isothermal no-slip conditions such as $v = 0$ and $T = 0$ were applied to the model, where v and T represent the velocity and temperature rise in the air. Two domains were used: the pressure acoustic domain and the thermoviscous domain for wave propagation in the labyrinthine structure. The acoustic domains are governed by the Helmholtz equation:

$$\nabla . \left(-\frac{1}{\rho} \nabla P \right) - \frac{\omega^2 P}{\rho c^2} = 0 \tag{1}$$

where P is the pressure, and ρ and c represent the density and speed of sound in the air, respectively. The governing equations of the thermoacoustic domain include the linearized Navier–Stokes (LNS) equation, the mass continuity equation, and the heat conduction equation [47]:

$$i\omega\rho v = \nabla . (-P_t I + \eta(\nabla v + (\nabla v)^T) - \frac{2}{3}\eta(\nabla . v) I) \tag{2}$$

$$i\omega\rho \left(\frac{P_t}{P_0} - \frac{T}{T_0} \right) + \rho \nabla . v = 0 \tag{3}$$

$$i\omega\rho C_p T = -\nabla . (-\kappa \nabla T) + i\omega\rho P_t \tag{4}$$

where v, P_t, T, C_p and I represent, respectively, the fluid velocity, Pressure, temperature variation, heat capacity of air at constant pressure and the identity matrix, $\eta = 1.814 \times 10^{-5} Pa.s$ is the dynamic viscosity coefficient and ω is angular frequency.

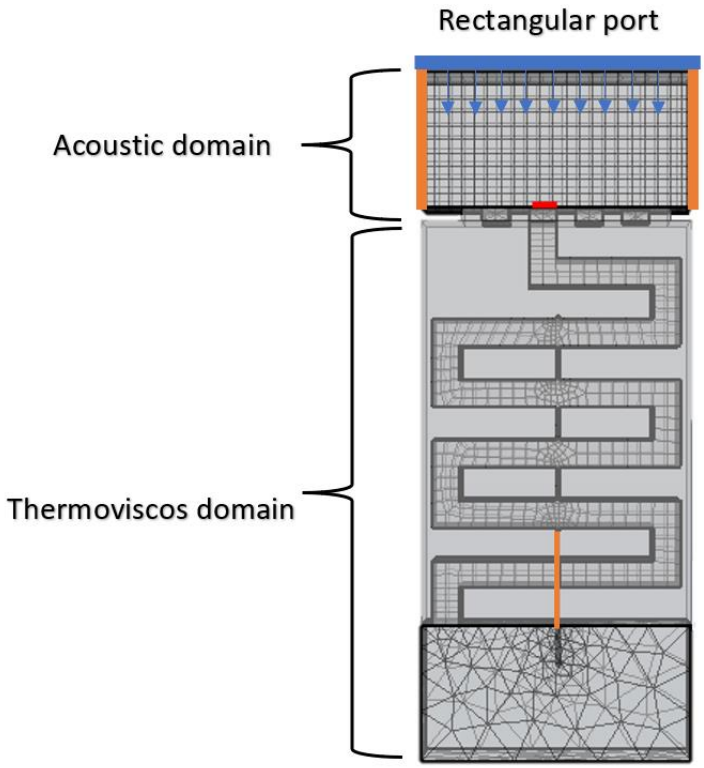

Figure 2*: Discretization of the model and domains*

A quadrilateral mesh was utilized for all domains. In Figure 2, the orange lines represent hard wall sound boundaries, while the blue line indicates the port boundary that releases a plane wave in the Z-direction. The red line marks the interaction point between the two physics.

The sound absorption coefficient, denoted as α, is calculated using the formula $\alpha = 1 - |R|^2$ where R is the ratio of the amplitude of the reflected sound wave to the amplitude of the incident sound wave. In this context, R quantifies the fraction of the incident wave that is reflected by the material. A higher absorption coefficient indicates more effective sound absorption, as it reflects a lower proportion of sound being reflected and a greater proportion being absorbed by the material. Thus, maximizing the absorption coefficient is essential for enhancing the sound attenuation properties of materials.

2.2. Experiments

The sound absorption coefficient of the specimens was evaluated using a cylindrical impedance tube with an internal diameter of 100 mm, corresponding to a cut-off frequency of 1600 Hz. Figure 3a shows the impedance tube used, while Figure 3b exhibits the parts of the impedance tube and the placement of the specimen within it.

(a)

(b)

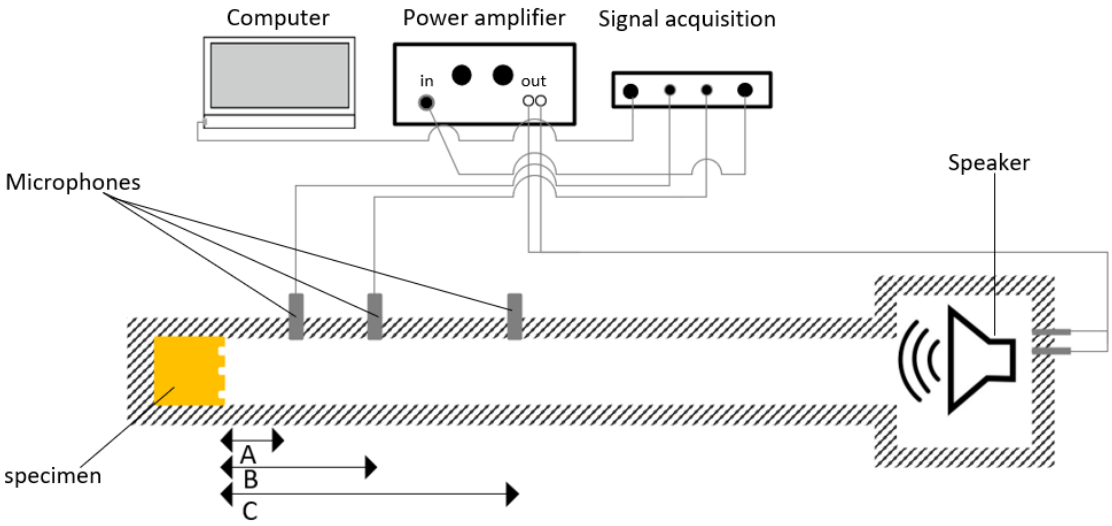

Figure 3*: (a) The impedance tube BSWA SW422 (b) the section of impedance tube and schematic of its components*

A physical sample for testing was created using the Fusion Deposition Modeling (FDM) additive manufacturing method. The specimen, composed of unit cells with six coiled-up spaces, was fabricated from durable Polylactic Acid (PLA) with a manufacturing resolution of 0.2 mm, a level of precision necessitated by the constraints of the impedance tube. The complete model consists of four part types: windows, a magazine, cells, and metal plates. The tested configuration used three cells held within the magazine, an arrangement that allows the windows to move without obstruction. A key design element for tunability is a slit within each cell that accommodates a 0.5 mm metal plate, which enables the operational mode to be changed. The components, assembly, and movement of the metal plate are visualized in Figure 4.

The experimental analysis of the sound absorption coefficient was conducted using a BSWA SW422 impedance tube. All measurements were performed in compliance with the ASTM E1050-24 standard, covering a frequency range of 63 Hz to 1600 Hz. A two-microphone technique was employed, with a frequency-dependent positioning strategy to ensure accuracy across the spectrum. As shown in Figure 3, microphones were placed at positions A and B for wideband measurements (63-500 Hz) and subsequently moved to positions A and C for the higher frequency range (400-1600 Hz).

(a) (b) (c) (d)

(e)

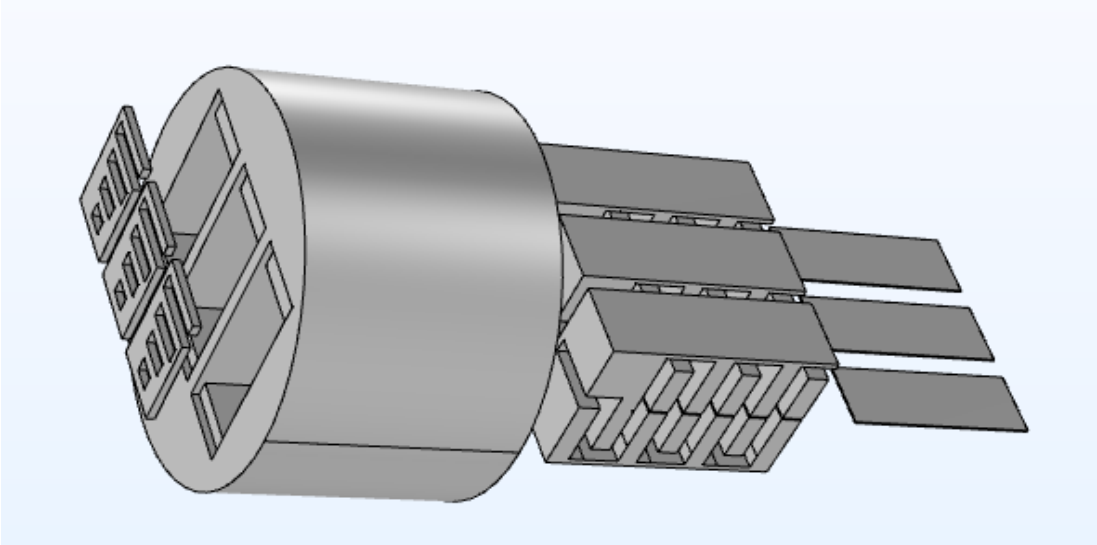

Figure 4*: (a) Bottom view of specimen (b) top view of specimen (c) the labyrinthine cell (d) 3D-view of labyrinthine cell with inserted metal plate, and (e) assembling of specimen windows, magazine, cells and metal plates*

For the experimental procedure, the test specimen was positioned at the end of the impedance tube, pressed against a solid, rigid wall. An amplifier-powered speaker located at the other end of the tube served as the sound source, generating acoustic waves at various frequencies.

To accurately capture data across a wide spectrum, a two-part measurement strategy was used, leveraging the three microphone positions available in the tube. First, for the low-frequency range of 60 Hz to 500 Hz, microphones were installed at positions A and B. Subsequently, for the high-frequency range of 400 Hz to 1600 Hz, the microphones were reconfigured to positions A and C.

This dual-setup approach ensures thorough frequency coverage for a precise analysis of the material's sound absorption properties. The deliberate 100 Hz overlap between the two measurement bands (from 400 Hz to 500 Hz) provides a crucial cross-check, enhancing the confidence and reliability of the final experimental data.

3. Results and discussion

3.1. Validation of the numerical model

A comparison of the results from the numerical simulations and the physical experiments is provided in Figure 5, while the 24 operational modes of the Adjustable Acoustic Labyrinthine Metamaterial (AALM) are illustrated in Figure 6.

During the initial analysis, significant discrepancies were observed between the experimental data and the numerical model. The source of this disagreement was identified as a physical imperfection in the experimental setup. Due to an extended portion of the internal metal plate, the test specimen could not sit perfectly flush against the rigid wall at the end of the impedance tube. This created an unintended air cavity behind the sample, allowing sound waves to enter a space that was not accounted for in the initial, ideal simulations (except for mode 1). Minor misalignments in the sample's diameter further ensured that this air gap affected all experimental modes, not just one.

To resolve this issue and align the simulation with the real-world conditions, the numerical model was updated. A 20-mm-thick cylindrical cavity, along with an airway into it, was added to the simulation for all modes. With this adjustment, the numerical predictions achieved excellent alignment with the measured experimental data. This entire process underscores a crucial point: precise dimensional control during the fabrication and assembly of test samples is paramount. It is essential for minimizing unintended variables, such as air gaps, to ensure that experimental results can be reliably validated against theoretical models.

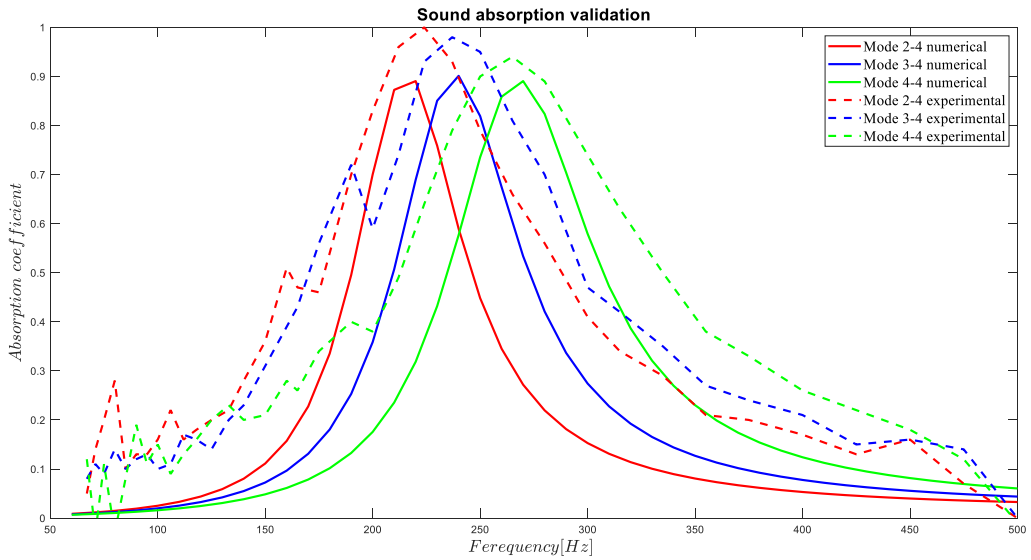

***Figure 5*: The validation of numerical models using experimental tests**

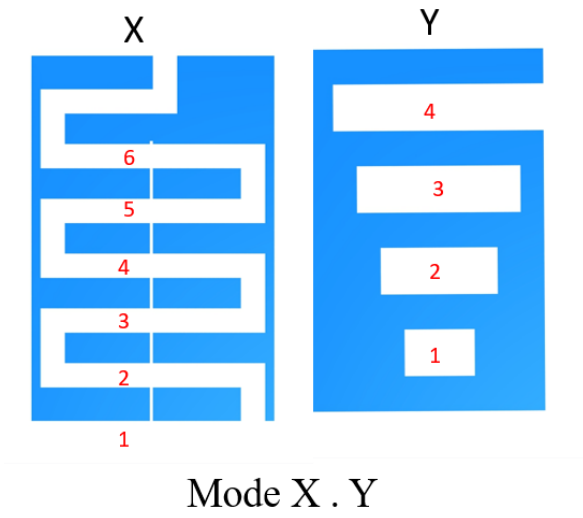

Figure 6 : Modes of AALM

The variation in the sound absorption coefficient due to changes in the position of the window was assessed using the impedance tube. Although the variation is minor at low frequencies, it is still observable. In Figure 7, four modes of the window test conducted in the impedance tube are shown. It can be seen that as the cross-section of the wave entrance is reduced, the frequency of maximum sound absorption decreases and shifts to lower frequencies. However, these changes are minor at low frequencies.

This observation suggests that the position and cross-section of the window play a crucial role in determining the frequency at which maximum sound absorption occurs. By reducing the cross-sectional area of the wave entrance, the effective length of the sound path is increased, which in turn lowers the resonance frequency. This effect is more pronounced at higher frequencies, where even small adjustments can lead to significant shifts in the absorption characteristics. These findings highlight the importance of precise control over the structural parameters of the metamaterial to achieve optimal sound absorption performance across a wide frequency range.

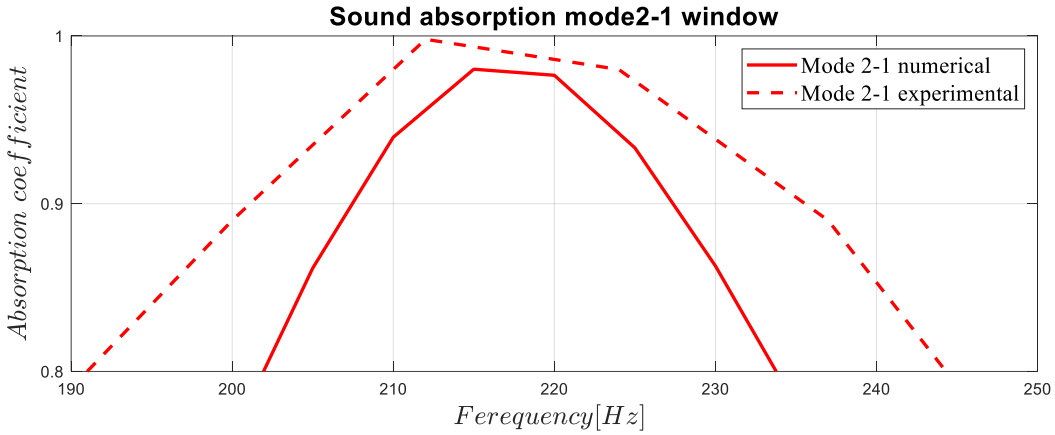
Sound absorption mode2-1 window
Mode 2-1 numerical
Mode 2-1 experimental
Absorption coefficient
Ferequency[Hz]
1
0.9
0.8
190
200
210
220
230
240
250

(a)

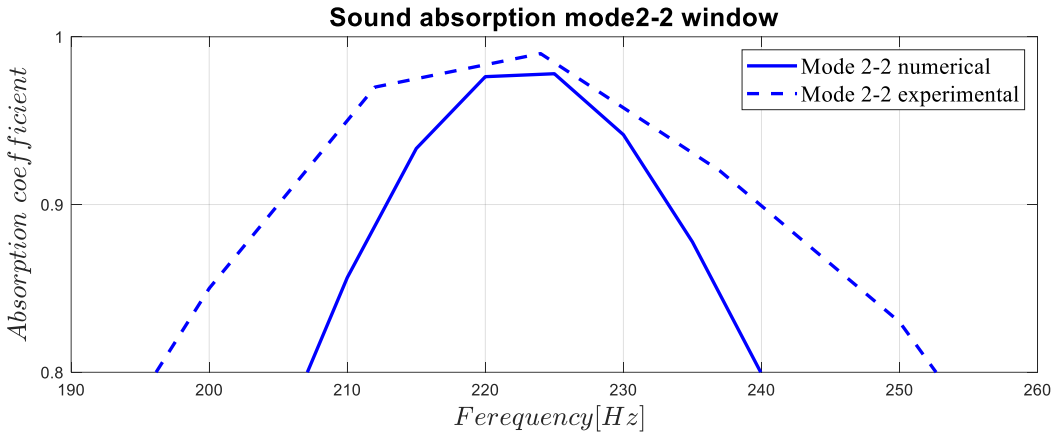
Sound absorption mode2-2 window
Mode 2-2 numerical
Mode 2-2 experimental
Absorption coefficient
Ferequency[Hz]
1
0.9
0.8
190
200
210
220
230
240
250
260

(b)

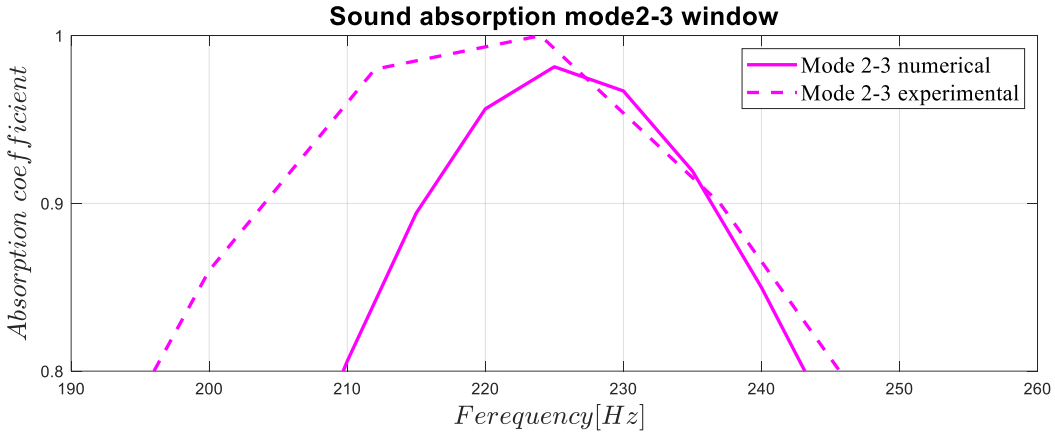
Sound absorption mode2-3 window
Mode 2-3 numerical
Mode 2-3 experimental
Absorption coefficient
Ferequency[Hz]
1
0.9
0.8
190
200
210
220
230
240
250
260

(c)

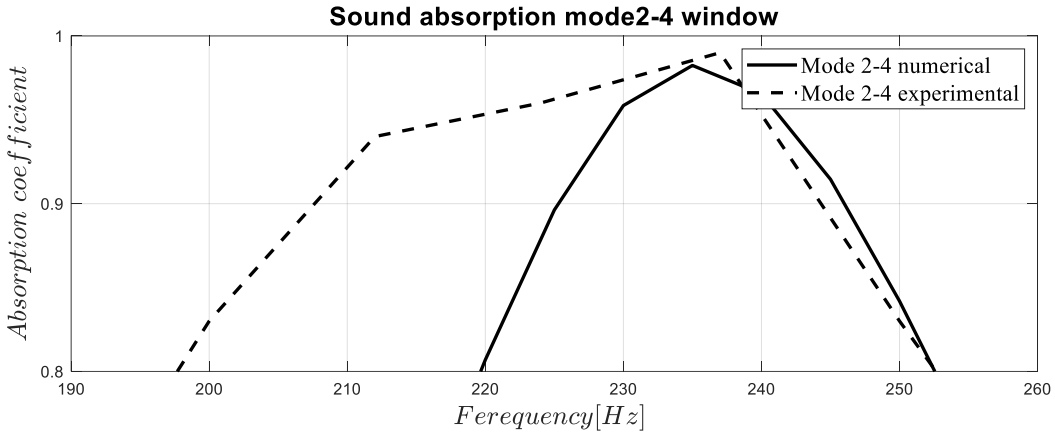

(d)

Figure 7*: (a) validation of mode 2-1, (b) validation of mode 2-2 (c) validation of mode 2-3 (d) validation of mode 2-4*

3.2. Results

The AALM incorporates six canal spaces and four distinct wave entrances. The number of canals can be reduced to one by repositioning the metal plate in the center, thereby decreasing the effective length. This reduction in effective length directly impacts sound absorption, as explained by acoustic impedance theory applied to labyrinth structures [34]. The formula defined by

$$\tilde{Z}_l(\omega) = -j\psi \sqrt{\frac{\tilde{\rho}_{eq}}{\tilde{C}_{eq}}} \cot\left(\omega\left(\sqrt{\tilde{\rho}_{eq}\,\tilde{C}_{eq}}\right)L_{eff}\right) \tag{5}$$

where $\psi = S_0/S_i$ is the area modifier factor that maintains the volume flow rate with $S_0 = WL$ and $S_i = ab$ Here, S_0 represents the XY-plane area of an individual cell, and S_i represents the cross-sectional area of the labyrinth spaces, respectively. Where $a = W - t$ and $b = [\,h - (n-1)t]/n$, with n is number of labyrinth canal, $l = L - 2b_0$ that is the length of canal space and the effective length approximately is

$$L_{eff} \approx \sqrt{F^2 + a^2} + \sqrt{l^2 + 3a^2} + \left((n-1)\left(\sqrt{l^2 + a^2}\right) + n\left(\sqrt{t^2 + a^2}\right)\right) \tag{6}$$

The L_{eff} is differ for mode1, because the effective length of end cavity add to effective length of labyrinth. Where calculated $L_{eff} - end = \acute{L} + \frac{2d}{\pi}$ where d is the depth of penetration for sound waves. $\tilde{\rho}_{eq}$represents the inertial and viscous contributions of the fluid and $\tilde{C}_{eq}$ comprises the thermal conductivity, and are the density and compressibility functions. They obtained by [48].

Changing the number of canals leads to different modes in the AALM. Mode one has the greatest effective length, and by adjusting the metal plate to increase the number of canals, the modes change. Mode six, however, has the least effective length. Table 1 displays the effective lengths in various modes and the corresponding parameter values, as illustrated in Figure 8.

Table 1: value of Parameters and effective length

Parameters	F	t	W	L	b_0	$\acute{L}$	d	a
Value [mm]	9.5	5	20	40	1.5	20	40	4

Modes	**n**	$\boldsymbol{L_{eff}}$[mm]
Mode 1	6	303.101
Mode 2	5	228.828
Mode 3	4	185.210
Mode 4	3	141.591
Mode 5	2	97.972
Mode 6	1	54.353

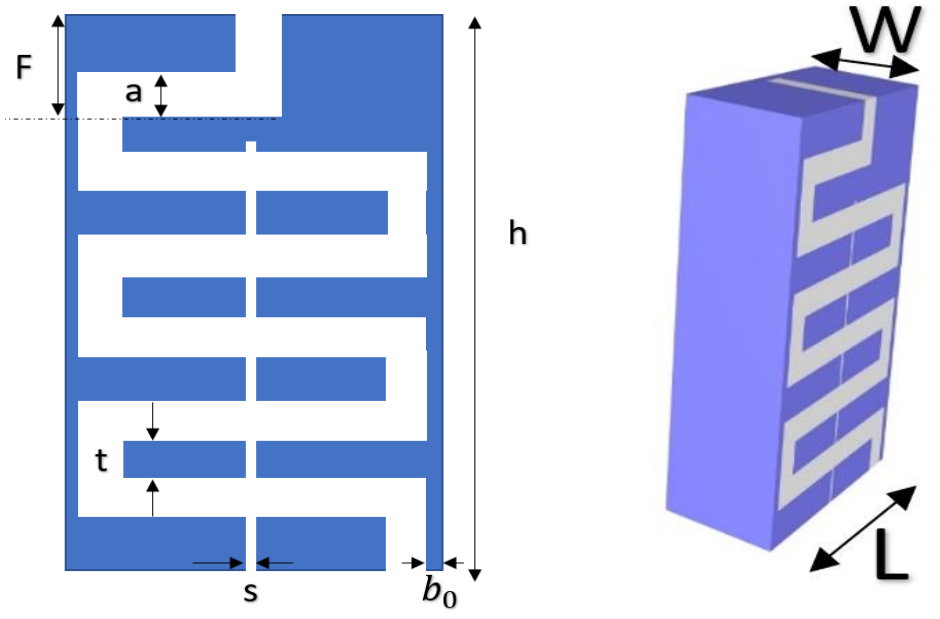

(a) **(b)**

Figure 8*: Schematic diagram of the cell Parameters Distribution.*

The performance of the Adjustable Acoustic Labyrinthine Metamaterial (AALM) is highly dependent on its selected operational mode, which allows it to be tuned for different acoustic conditions. The principle of maximum sound absorption is achieved when a material's acoustic impedance has a real part of zero and an imaginary part of one; the specific frequency at which this condition is met varies for each mode. The complex relationship between the absorption coefficient, frequency, and the chosen mode is visually detailed in Figure 8 and Figure 9, highlighting the importance of mode-specific analysis.

The physical mechanism for changing between modes is the position of a 0.5 mm thick stainless-steel plate, which is housed within a slit (depicted in Figure 4) and acts as a movable barrier within the labyrinth. The plate's position relative to the top of the model (parameter A) dictates the active mode. As shown in Figure 5(g), the plate position directly correlates with changes in the absorption coefficient. Mode 1 is set at a position of -59 mm, with each subsequent mode engaged by shifting the plate 9 mm, culminating in mode 6 at -14 mm. The full sequence of positions for modes 1 through 6 is -59 mm, -50 mm, -41 mm, -32 mm, -23 mm, and -14 mm, respectively.

Each of these physical positions yields a distinct acoustic performance. The frequency of maximum sound absorption shifts significantly across the modes: 240 Hz (mode 1), 450 Hz (mode 2), 540 Hz (mode 3), 680 Hz (mode 4), 920 Hz (mode 5), and 1620 Hz (mode 6). The efficiency also changes, with the absorption coefficient starting near a perfect value of approximately 1 in mode 1 and decreasing to 0.56 by mode 6. The overall analysis was performed within a 60-2000 Hz frequency range, a scope broad enough to capture important features like the second resonance peaks of the initial modes and demonstrate the AALM's wide-spectrum capabilities.

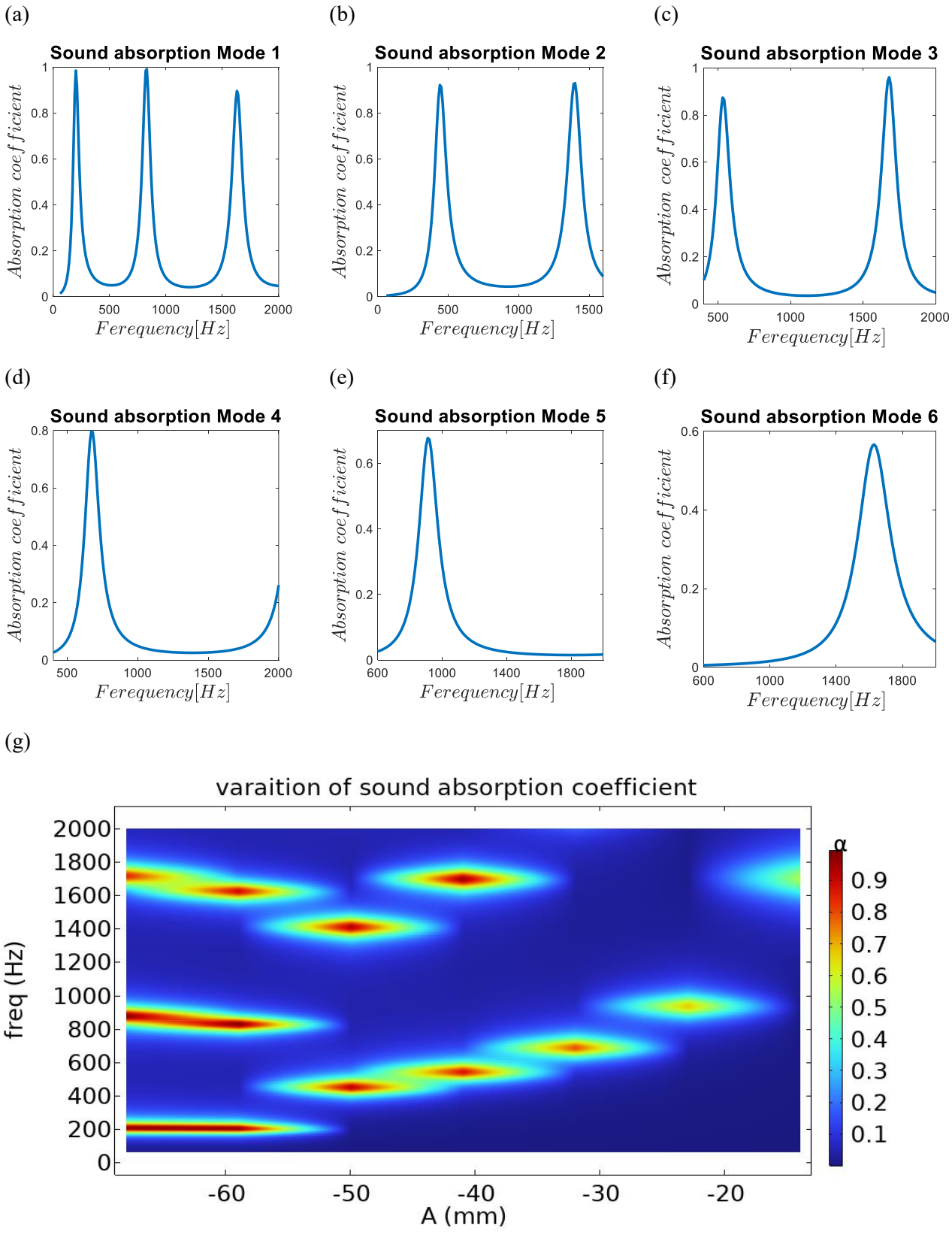

Figure 9*: (a) sound absorption coefficient in mode 1 (b) sound absorption coefficient in mode 2 (c)*

sound absorption coefficient in mode 3 (d) sound absorption coefficient in mode 4 (e) sound absorption coefficient in mode 5 (f) sound absorption coefficient in m

In addition to its primary tuning system, the sound absorption capabilities of the Adjustable Acoustic Labyrinthine Metamaterial (AALM) can be further refined using a component known as the "window." This feature serves as a tunable neck for the wave entrance, offering precise control over the sound absorption frequency. The operational principle is based on the Helmholtz equation: by adjusting the cross-sectional area of the window's opening, the acoustic properties of the model can be modified. Specifically, reducing the entrance area allows the AALM to absorb longer wavelengths, which shifts the peak absorption coefficient to a lower frequency.

This adjustability is implemented through four distinct operational modes for the window, each defined by a unique geometric configuration of the entrance neck. Figure 10 provides a schematic of this tunable window, while Table 2 summarizes the specific dimensions for each of the four modes, where *a* represents the entrance width and *b* represents its length. The ability to dynamically alter these dimensions provides a versatile and sophisticated method for tailoring the AALM's acoustic response, making it highly adaptable for targeted frequency control in diverse applications.

(a) (b)

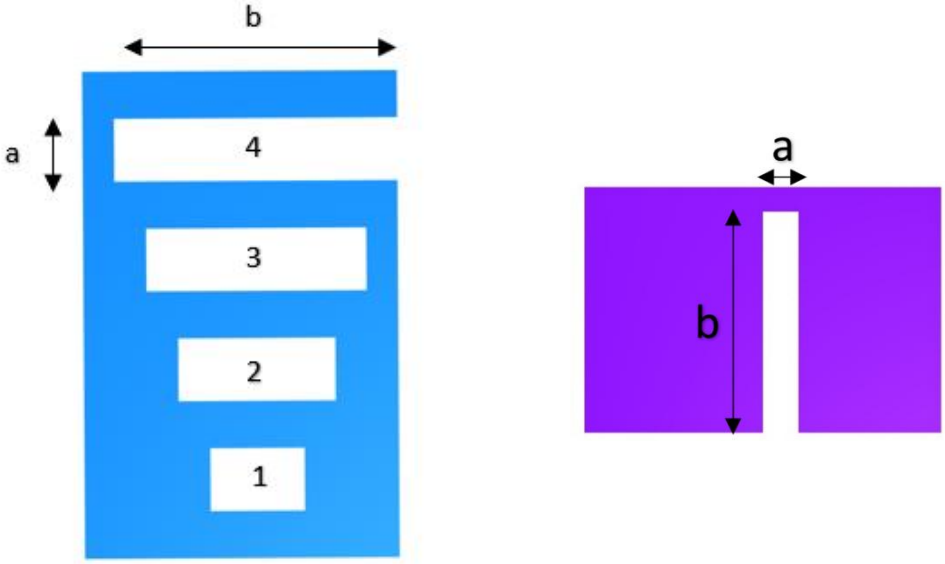

Figure 10*: (a) the front view of window and specification of modes on different entrance (b) up-view of cell and specification dimension*

Table 2: dimension of window modes

Modes	**b [mm]**	**S [mm^2]**
Mode 1	6	24
Mode 2	10	40
Mode 3	14	56
Mode 4	18	72

Adjusting the window configuration provides a method for fine-tuning the AALM's sound absorption, though the resulting frequency variations are smaller than those achieved by altering the number of canals. As an example, within the four-canal configuration, changing the window mode shifts the peak absorption frequency by approximately 10 Hz. For this specific case, the maximum absorption frequencies for the four window modes occur at 490 Hz, 520 Hz, 530 Hz, and 540 Hz, respectively. Figure 11(a) illustrates the sound absorption performance for the four window modes across each of the available canal configurations, while Figure 11(b) isolates the variation in the absorption coefficients.

The physical mechanism for this adjustment is the position of the window (parameter `cc`), which moves in 7 mm increments to change the mode. The positions corresponding to modes one through four are -13 mm, -6 mm, 1 mm, and 8 mm. This dynamic adjustment allows for precise control of the sound absorption properties.

Ultimately, the AALM's design incorporates two layers of tunability. The six modes available from changing the number of canals provide major adjustments, while the four modes from adjusting the window's cross-section offer fine-tuning. This combination yields a total of 24 distinct operational modes. Such versatility allows the AALM to achieve highly efficient sound absorption across a broad and continuous range of frequencies.

(a)

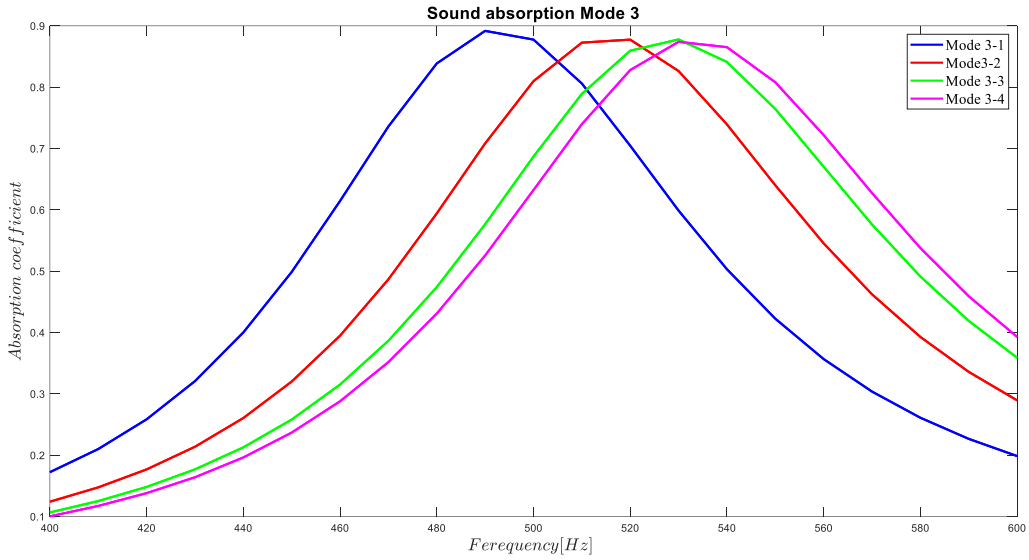

(b)

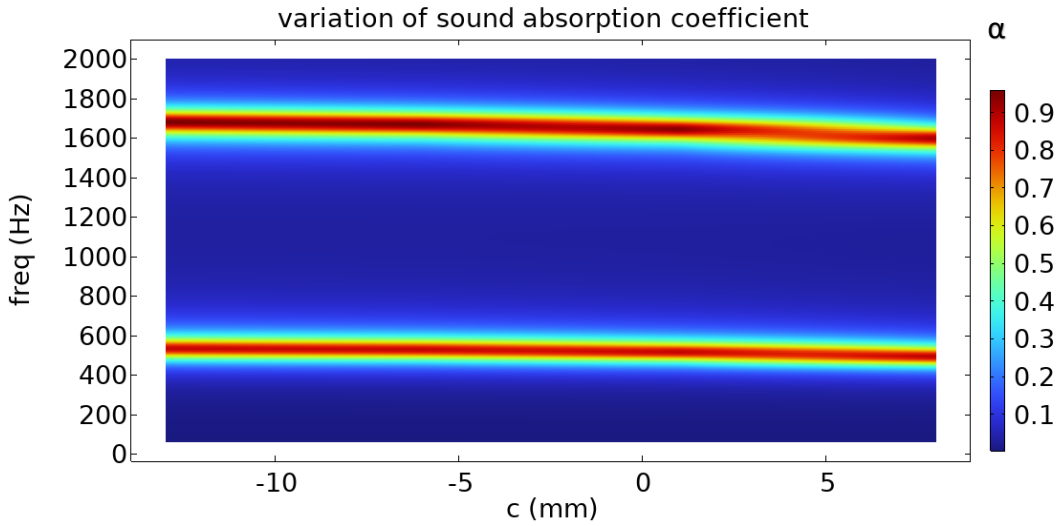

Figure 11*: (a) sound absorption coefficient for different wave entrance for mode 3 (b) contour of variation of absorption coefficient by moving window*

The modes are illustrated in Figure 11(a). Initially, canal modes are addressed, followed by window modes. Mode 1-1 corresponds to the lowest frequency for sound absorption, while Mode 6-4 corresponds to the highest frequency. In both cases, as the number of modes increases, the frequency of maximum absorption also increases. The AALM sound absorption can be modified by altering the canal modes, and for minor adjustments, the window modes can be changed. This innovation approximately covers the entire range of [220 Hz-2000 Hz], offering superior

performance compared to conventional materials like porous materials. This is due to the fact that each mode achieves maximum sound absorption, with most modes nearing a perfect sound absorption coefficient.

4. Conclusion

This study introduces the Adjustable Acoustic Labyrinthine Metamaterial (AALM), a novel sound absorber designed to provide near-perfect, tunable absorption across a wide range of frequencies. The AALM's performance was thoroughly investigated using a dual approach. First, its 24 operational modes were modeled numerically using the Finite Element Method (FEM) in COMSOL Multiphysics, incorporating both pressure acoustic and thermoviscous domains. Second, physical specimens were created using Fused Deposition Modeling (FDM), and experimental tests on six of these modes in an impedance tube produced results that showed acceptable agreement with the simulations.

The research included sensitivity analyses to determine how the sound absorption coefficient and target frequencies respond to changes in the two primary tuning parameters: the number of coiled spaces and the cross-section of the wave-entrance. The study also explored the dynamics of energy dissipation and thermoviscous performance across different modes. An important secondary finding was related to the air slits within the cells; it was discovered that some short wavelengths bypass the main labyrinth, which increases the structure's effective length and pushes the absorption frequency higher, enhancing the absorption coefficient in that range.

Based on these comprehensive findings, this work establishes the AALM as a novel and highly adaptable acoustic metamaterial, validating its effectiveness for absorbing noise across a targeted, broad frequency spectrum.

References

1. Gao, N., Z. Zhang, J. Deng, X. Guo, B. Cheng, and H. Hou, *Acoustic metamaterials for noise reduction: a review.* Advanced Materials Technologies, 2022. **7**(6): p. 2100698.
2. Hansen, C.H., *Current and future industrial applications of active noise control.* Noise Control Engineering Journal, 2005. **53**(5): p. 181-196.
3. Gabbert, U., F. Duvigneau, and S. Ringwelski, *Noise control of vehicle drive systems.* Facta Universitatis, Series: Mechanical Engineering, 2017. **15**(2): p. 183-200.

4. Gabor, R.-M., P. Blaga, and B.-M. Caseriu, *Quantitative analysis of predictors of acoustic materials for noise reduction as sustainable strategies for materials in the automotive industry.* 2024.
5. Sadeghian, M., *Technologies for aircraft noise reduction: A review.* Journal of Aeronautics & Aerospace Engineering, 2020.
6. Lockard, D.P. and G.M. Lilley, *The airframe noise reduction challenge*. 2004.
7. Hedayati, R. and S. Lakshmanan, *Pneumatically-Actuated Acoustic Metamaterials Based on Helmholtz Resonators.* Materials, 2020. **13**(6): p. 1456.
8. Hedayati, R., A. Rubio Carpio, S. Luesutthiviboon, D. Ragni, F. Avallone, D. Casalino, and S. van der Zwaag, *Role of polymeric coating on metallic foams to control the aeroacoustic noise reduction of airfoils with permeable trailing edges.* Materials, 2019. **12**(7): p. 1087.
9. Muhammad and C. Lim, *From photonic crystals to seismic metamaterials: A review via phononic crystals and acoustic metamaterials.* Archives of Computational Methods in Engineering, 2022. **29**(2): p. 1137-1198.
10. Ang, L.Y.L., F. Cui, K.-M. Lim, and H.P. Lee, *A systematic review of emerging ventilated acoustic metamaterials for noise control.* Sustainability, 2023. **15**(5): p. 4113.
11. Hedayati, R. and S.P. Lakshmanan, *Active acoustic metamaterial based on Helmholtz resonators to absorb broadband low-frequency noise.* Materials, 2024. **17**(4): p. 962.
12. Hedayati, R. and M. Bodaghi, *Acoustic metamaterials and acoustic foams: recent advances.* Applied Sciences, 2022. **12**(6): p. 3096.
13. Hedayati, R., Y. Sheikhnejad, and M.M. Aghdam, *Editorial to the special issue on advanced micro/nanoscale porous materials for novel applications: answering to future needs.* Transport in Porous Media, 2022. **142**(1): p. 1-4.
14. Rastegar, N., A. Ershad-Langroudi, H. Parsimehr, and G. Moradi, *Sound-absorbing porous materials: a review on polyurethane-based foams.* Iranian Polymer Journal, 2022: p. 1-23.
15. Allard, J. and N. Atalla, *Propagation of sound in porous media: modelling sound absorbing materials*. 2009: John Wiley & Sons.
16. Hedayati, R., S. Van Der Zwaag, F. Avallone, D. Casalino, and D. Ragni, *Acoustic Liner* 2018.
17. Maa, D.-Y., *Potential of microperforated panel absorber.* the Journal of the Acoustical Society of America, 1998. **104**(5): p. 2861-2866.
18. Li, D., D. Chang, and B. Liu, *Enhanced low-to mid-frequency sound absorption using parallel-arranged perforated plates with extended tubes and porous material.* Applied Acoustics, 2017. **127**: p. 316-323.
19. Tang, P. and W. Sirignano, *Theory of a generalized Helmholtz resonator.* Journal of Sound and Vibration, 1973. **26**(2): p. 247-262.
20. Fok, L., M. Ambati, and X. Zhang, *Acoustic metamaterials.* MRS bulletin, 2008. **33**(10): p. 931-934.
21. Zhao, X., L. Cai, D. Yu, Z. Lu, and J. Wen, *A low frequency acoustic insulator by using the acoustic metasurface to a Helmholtz resonator.* AIP Advances, 2017. **7**(6).
22. Cummer, S.A., J. Christensen, and A. Alù, *Controlling sound with acoustic metamaterials.* Nature Reviews Materials, 2016. **1**(3): p. 1-13.
23. Rafique, F., J.H. Wu, M. Waqas, X. Lushuai, and F. Ma, *A thin double-layer multiple parallel-arranged inhomogeneous microperforated panel absorber for wideband low-frequency sound absorption.* Journal of the Brazilian Society of Mechanical Sciences and Engineering, 2022. **44**: p. 1-18.
24. Catapane, G., G. Petrone, O. Robin, and K. Verdière, *Coiled quarter wavelength resonators for low-frequency sound absorption under plane wave and diffuse acoustic field excitations.* Applied Acoustics, 2023. **209**: p. 109402.

25. Li, J., L. Fok, X. Yin, G. Bartal, and X. Zhang, *Experimental demonstration of an acoustic magnifying hyperlens.* Nature materials, 2009. **8**(12): p. 931-934.
26. Faure, C., O. Richoux, S. Félix, and V. Pagneux, *Experiments on metasurface carpet cloaking for audible acoustics.* Applied Physics Letters, 2016. **108**(6).
27. Fang, N., D. Xi, J. Xu, M. Ambati, W. Srituravanich, C. Sun, and X. Zhang, *Ultrasonic metamaterials with negative modulus.* Nature materials, 2006. **5**(6): p. 452-456.
28. Li, J. and C.T. Chan, *Double-negative acoustic metamaterial.* Physical Review E—Statistical, Nonlinear, and Soft Matter Physics, 2004. **70**(5): p. 055602.
29. Almeida, G.d.N., E.F. Vergara, L.R. Barbosa, and R. Brum, *Low-frequency sound absorption of a metamaterial with symmetrical-coiled-up spaces.* Applied Acoustics, 2021. **172**: p. 107593.
30. Xie, Y., W. Wang, H. Chen, A. Konneker, B.-I. Popa, and S.A. Cummer, *Wavefront modulation and subwavelength diffractive acoustics with an acoustic metasurface.* Nature communications, 2014. **5**(1): p. 5553.
31. Xie, Y., B.-I. Popa, L. Zigoneanu, and S.A. Cummer, *Measurement of a broadband negative index with space-coiling acoustic metamaterials.* Physical review letters, 2013. **110**(17): p. 175501.
32. Liang, Z. and J. Li, *Extreme acoustic metamaterial by coiling up space.* Physical review letters, 2012. **108**(11): p. 114301.
33. Catapane, G., D. Magliacano, G. Petrone, A. Casaburo, F. Franco, and S. De Rosa. *Labyrinth resonator design for low-frequency acoustic meta-structures*. in *International Conference on Wave Mechanics and Vibrations*. 2022. Springer.
34. Wang, Y., H. Zhao, H. Yang, J. Zhong, and J. Wen, *A space-coiled acoustic metamaterial with tunable low-frequency sound absorption.* Europhysics Letters, 2018. **120**(5): p. 54001.
35. Setaki, F., F. Tian, M. Turrin, M. Tenpierik, L. Nijs, and A. Van Timmeren, *3D-printed sound absorbers: Compact and customisable at broadband frequencies.* Architecture, Structures and Construction, 2023. **3**(2): p. 205-215.
36. Roudbarian, N., M. Baniasadi, P. Nayyeri, M. Ansari, R. Hedayati, M.J.S.M. Baghani, and Structures, *Enhancing shape memory properties of multi-layered and multi-material polymer composites in 4D printing.* 2021. **30**(10): p. 105006.
37. Hedayati, R., N. Ghavidelnia, M. Sadighi, and M. Bodaghi, *Improving the accuracy of analytical relationships for mechanical properties of permeable metamaterials.* Applied Sciences, 2021. **11**(3): p. 1332.
38. Ghanati, G. and S. Azadi, *Active control of vehicle's interior sound field by using multichannel H∞ robust controller.* Proceedings of the Institution of Mechanical Engineers, Part D: Journal of Automobile Engineering, 2020. **234**(2-3): p. 725-738.
39. Pei, C.M., J.T. Liu, Z.Y. Liu, and L.M. Ying, *The design of active noise control system in power transformer.* Applied Mechanics and Materials, 2013. **364**: p. 275-279.
40. Sharafkhani, N., *A Helmholtz resonator-based acoustic metamaterial for power transformer noise control.* Acoustics Australia, 2022. **50**(1): p. 71-77.
41. Almeida, G.d.N., E.F. Vergara, L.R. Barbosa, A. Lenzi, I. Cassettari, and R.Z. Mikulski, *Sound absorption performance of a labyrinthine metamaterial with arbitrary cross-sectional microperforations.* Journal of the Brazilian Society of Mechanical Sciences and Engineering, 2023. **45**(11): p. 607.
42. Pavan, G. and S. Singh, *Near-perfect sound absorptions in low-frequencies by varying compositions of porous labyrinthine acoustic metamaterial.* Applied Acoustics, 2022. **198**: p. 108974.
43. Zhang, W. and F. Xin, *Coiled-up structure with porous material lining for enhanced sound absorption.* International Journal of Mechanical Sciences, 2023. **256**: p. 108480.

44. Bijsterveld, K., E. Cleophas, S. Krebs, and G. Mom, *Sound and safe: A history of listening behind the wheel*. 2014: Oxford University Press, USA.
45. Akl, W. and A. Baz, *Multi-cell active acoustic metamaterial with programmable bulk modulus.* Journal of intelligent material systems and structures, 2010. **21**(5): p. 541-556.
46. Pope, S. and H. Laalej, *A multi-layer active elastic metamaterial with tuneable and simultaneously negative mass and stiffness.* Smart Materials and Structures, 2014. **23**(7): p. 075020.
47. Meng, H., M.-A. Galland, M. Ichchou, O. Bareille, F. Xin, and T. Lu, *Small perforations in corrugated sandwich panel significantly enhance low frequency sound absorption and transmission loss.* Composite Structures, 2017. **182**: p. 1-11.
48. Stinson, M.R., *The propagation of plane sound waves in narrow and wide circular tubes, and generalization to uniform tubes of arbitrary cross-sectional shape.* The Journal of the Acoustical Society of America, 1991. **89**(2): p. 550-558.